Journal of Materials Chemistry B

ROYAL SOCIETY OF CHEMISTRY

PAPER

View Article Online
View Journal | View Issue

Cite this: J. Mater. Chem. B, 2022, 10, 6688

Molecularly imprinted polymer nanogels targeting the HAV motif in cadherins inhibit cell–cell adhesion and migration†

Paulina X. Medina Rangel,‡*[a] Alejandra Mier,[a] Elena Moroni,[a] Franck Merlier,[a] Levi A. Gheber,[b] Razi Vago,[b] Irene Maffucci,[a] Bernadette Tse Sum Bui *[a] and Karsten Haupt *[a]

Cadherins are cell–surface proteins that mediate cell–cell adhesion. By regulating their grip formation and strength, cadherins play a pivotal role during normal tissue morphogenesis and homeostasis of multicellular organisms. However, their dysfunction is associated with cell migration and proliferation, cancer progression and metastasis. The conserved amino acid sequence His-Ala-Val (HAV) in the extracellular domain of cadherins is implicated in cadherin-mediated adhesion and migration. Antagonists of cadherin adhesion such as monoclonal antibodies and small molecule inhibitors based on HAV peptides, are of high therapeutic value in cancer treatment. However, antibodies are not stable outside their natural environment and are expensive to produce, while peptides have certain limitations as a drug as they are prone to proteolysis. Herein, we propose as alternative, a synthetic antibody based on molecularly imprinted polymer nanogels (MIP-NGs) to target the HAV domain. The MIP-NGs are biocompatible, have high affinity for N-cadherin and inhibit cell adhesion and migration of human cervical adenocarcinoma (HeLa) cells, as demonstrated by cell aggregation and Matrigel invasion assays, respectively. The emergence of MIPs as therapeutics for fighting cancer is still in its infancy and this novel demonstration reinforces the fact that they have a rightful place in cancer treatment.

Received 28th March 2022,
Accepted 8th May 2022

DOI: 10.1039/d2tb00680d

rsc.li/materials-b

Introduction

Cadherins are a large family of cell-surface transmembrane glycoproteins that mediate Ca^{2+}-dependent cell-cell adhesion.[1] Cadherin-mediated adhesion plays a central role in tissue morphogenesis during embryonic development, maintenance of tissue and organ architecture, cell motility and gene expression.[2] However, the dysfunction of these molecules due to various pathological conditions is implicated in uncontrolled cell migration and proliferation, tumour and metastatic cancer progression.[3–6] Type I classical cadherins which comprise E (epithelial), N (neural) and P (placental) cadherins are characterized by their five ectodomains (EC1-EC5), a conserved tryptophan residue localized at the second position (Trp2) at the N-terminal and a conserved His-Ala-Val (HAV) sequence in the EC1 ectodomain[2,7] (Fig. 1A). Cadherin-mediated cell-cell adhesion occurs *via* the reciprocal insertion of Trp2 from one cadherin into the hydrophobic pocket, lined by the conserved HAV domain of an identical cadherin from an adjacent cell.

To fight cancer development and metastasis, E-, N- and P-cadherins have served as viable therapeutic targets for numerous antibodies[5,8,9] and small molecule inhibitors.[10] The therapeutic antibodies were directed towards various epitopes on the extracellular domain and a few have been tested in preclinical studies.[11,12] Regarding small molecule inhibitors, peptides containing the cell adhesion recognition sequence HAV have been used principally as N-cadherin antagonists.[10,13] For instance, the cyclic peptide N-Ac-CHAVC-NH_2, known as ADH-1 and developed by Adherex Technologies Inc., has successfully completed a number of phase I and II clinical trials, for its ability to inhibit tumour growth when used alone[14] or in combination with anti-cancer drugs.[15] Importantly, the amino acids that flank the HAV domain determine both the specificity and the activity of the peptides. Consequently, several peptides that act as N-cadherin inhibitors have been

[a] CNRS Enzyme and Cell Engineering Laboratory, Université de Technologie de Compiègne, Rue du Docteur Schweitzer, CS 60319, 60203 Compiègne Cedex, France. E-mail: paulina.medinarangel@yale.edu, jeanne.tse-sum-bui@utc.fr, karsten.haupt@utc.fr

[b] The Avram and Stella Goldstein-Goren Department of Biotechnology Engineering, Ben-Gurion University of the Negev, P.O. Box 653, Beer-Sheva 84105, Israel

† Electronic supplementary information (ESI) available. See DOI: https://doi.org/10.1039/d2tb00680d

‡ Present address: Department of Internal Medicine, Yale University School of Medicine, New Haven, Connecticut, USA.

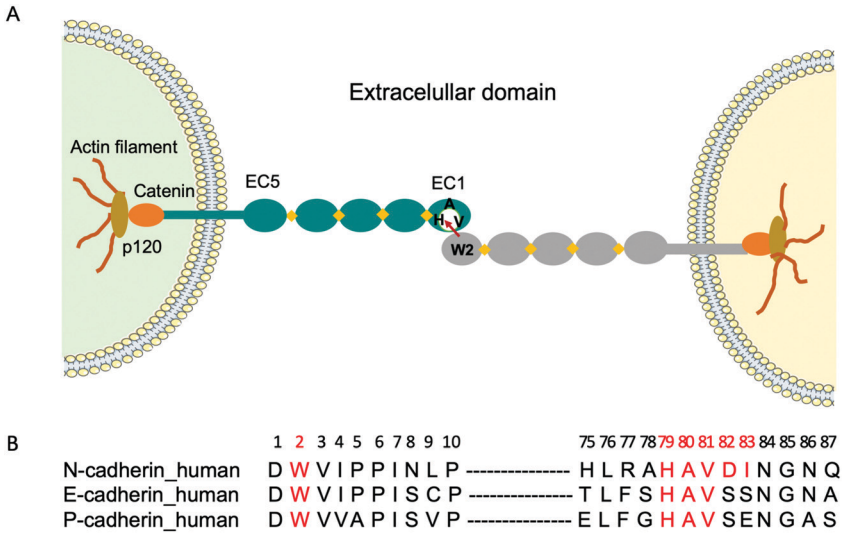

Fig. 1 (A) Schematic representation of trans dimerization of cadherins. The five ectodomains (EC1 to EC5) are represented as grey and green ovals, and Ca^{2+} ions are shown as yellow rhombi. Adhesion occurs by the insertion of W2 from one cadherin into the hydrophobic pocket, lined by HAV located in the EC1 of the adjacent cadherin. (B) Multiple sequence alignment showing the amino acids (red) in human E-, N- and P-cadherins, involved in cell adhesion. Alignment performed with EMBL-EBI.

synthesized by incorporating flanking amino acids specific to N-cadherin to the HAV peptide. One of the first reported peptides with this purpose is the linear decapeptide *N*-Ac-LRAHAVDING-NH_2, that inhibits human N-cadherin in neurite outgrowth.[16] More recently, a shorter cyclic peptide containing the HAVDI sequence[13,17] was identified as a highly potent inhibitor of N-cadherin cell adhesion and cell differentiation. It was also shown that when the HAV motif is flanked by a single serine, which mimics the natural HAVS sequence of E-cadherin, it loses its ability to inhibit the N-cadherin response, underlining the high specificity of interaction. However, peptides have certain limitations as a drug, as they are prone to proteolysis. As an alternative, we propose to use molecularly imprinted polymer nanogels (MIP-NGs) as synthetic antibodies to target the HAVDI domain, for blocking N-cadherin adhesion.

Molecularly imprinted polymers (MIPs) are tailor-made synthetic antibodies possessing specific cavities designed for a target molecule.[18–20] They are obtained by polymerizing functional and crosslinking monomers around the molecule of interest which acts as a template. After polymerization, the template is removed, resulting in a polymer with binding sites that are complementary in size, shape, and position of the functional groups to the template. The MIP can subsequently recognize and bind the molecule of interest with high affinity and specificity similar to that of an antibody with its antigen. Recently, we showed that MIP-NGs targeting the conserved N-terminal epitope Asp1-Trp2-Val3-Ile4-Pro5-Pro6-Ile7 (DWVIPPI) (Fig. 1B) had high selectivity and affinity for E- and N-cadherins. Consequently, they could inhibit cell-cell adhesion in cell aggregation assays, disrupt three-dimensional tumour spheroids and prevent the invasion of human cervical adenocarcinoma (HeLa) cells in Matrigel invasion assays.[21] Thus MIP-NGs are very promising to function as therapeutic drugs,[22,23] especially they seem to be stronger inhibitors than small molecule inhibitors, probably because they can cover large surface areas at the protein-protein interfaces. While both E- and N-cadherins can be involved in cancer development depending on the cell and tissue type, we wanted to explore the possibility of targeting preferentially one of the subtypes. Since the DWVIPPI epitope is common to E- and N-cadherins, we opted for the second epitope involved in the cadherin-mediated interaction, containing the HAV sequence, which shows some subtype specificity (Fig. 1B). Our present results show that the MIP-NGs targeting the HAVDI domain have higher affinities for N-cadherin than the small HAV-based peptide antagonists reported in the literature, and that they can specifically inhibit N-cadherin cell adhesion and invasion, as evaluated in cell aggregation and Matrigel invasion assays, respectively.

Results and discussion

Solid-phase synthesis of MIP-NGs

As reported above, the strongest inhibitor of N-cadherin adhesion, based on the HAV sequence is a cyclic peptide inhibitor composed of HAVDI.[13] Herein, the main challenge is to obtain a synthetic antibody able to recognize the HAVDI sequence (Fig. 1B and 2A), which is an internal peptide. We selected the sequence AHAVDING as epitope, complemented with two cysteine residues at both ends for cyclisation, so as to closely mimic the conformation of the HAVDI peptide (Fig. 2B).[24] The final cyclic template peptide, CAHAVDINGC-K(N_3) (C-C) contains a modified lysine residue bearing an azide moiety for the immobilization of the template *via* click chemistry.[25] The 3D structure of the free template epitope, flanked by 2 Cys (Fig. 2C, violet) was predicted with PEP-FOLD2 and superposed onto the

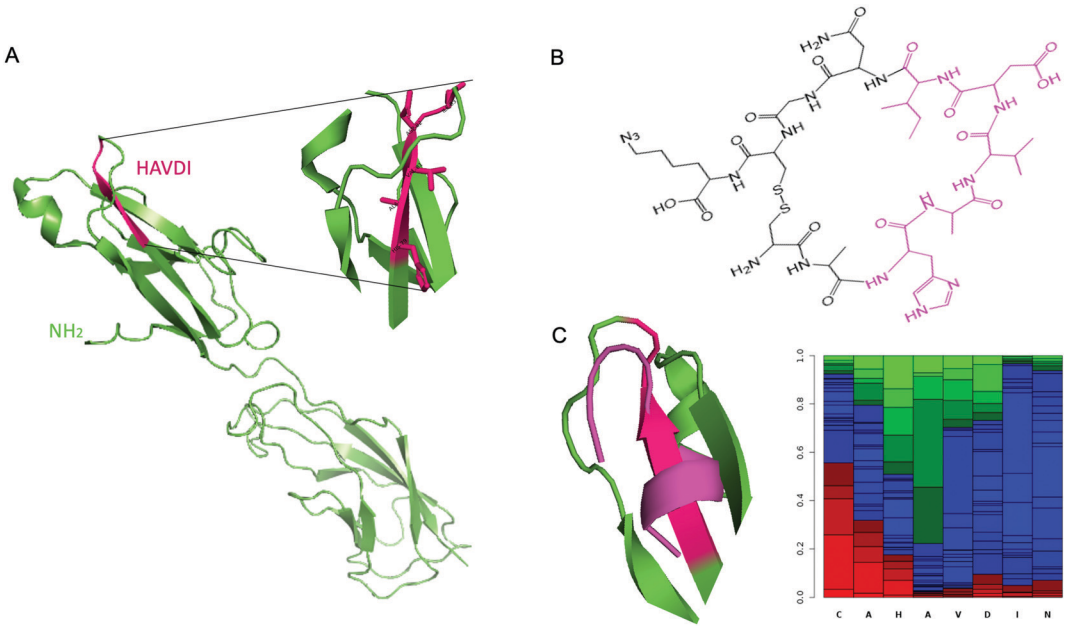

Fig. 2 (A) Crystal structure of murine N-cadherin domains EC 1–2 (PDB accession code 2QVI). Murine N-cadherin has 96% identity with human N-cadherin.[30] The sequence HAVDI is highlighted in fuchsia (B) Chemical structure of cyclic template peptide NH_2-CAHAVDINGCK(N_3)-COOH. (C) (Left) Superposition of the predicted 3D structure of the template peptide (flanked by 2 Cys) (violet), onto the native protein epitope. (Right) PEP-FOLD2 prediction of secondary structures probabilities associated to the cyclic template amino acids residues. Green: extended, blue: coil and red: helix.

native protein with PyMol. PEP-FOLD2 indicates a progressive increase in an extended secondary structure preference up to alanine in position 4 (0.8) followed by a prevalence of an unstructured conformation, which is coherent with the conformation in the native protein.

MIPs were produced by a solid-phase synthesis approach,[26–28] where the template molecule is covalently immobilized on glass beads (GBs) as solid support (Fig. 3). This configuration allows an oriented immobilization of the epitope upon which polymer nanogels are synthesized. The binding sites of the resulting MIPs all have the same orientation, thus MIPs synthesized by the solid-phase approach can be considered analogous to monoclonal antibodies. Prior to MIP synthesis, GBs were first activated by boiling in NaOH to introduce -OH groups. After activation, they were functionalized with *O*-(propargyloxy)-*N*-(triethoxysilylpropyl)urethane to introduce terminal alkyne groups.[29] The template peptide, functionalized with an azide moiety was immobilized on the alkyne-derivatized GBs through a copper(I)-catalyzed alkyne-azide cycloaddition (CuAAC). Click chemistry offers the advantage that the peptide is immobilized without compromising the amino acid side chains that play a crucial role during the imprinting process.

To synthesize the MIP-NGs, a mixture of monomers capable of interacting with the amino acid side chains of the peptide, was employed. *N*-Isopropylacrylamide (NIPAM) constituted the major monomer to yield thermoresponsive polymers that can be easily released from the support by changing the temperature.[25–27] *N-tert*-butyl acrylamide (TBAM) was used to target the hydrophobic amino acids. A benzamidine-based

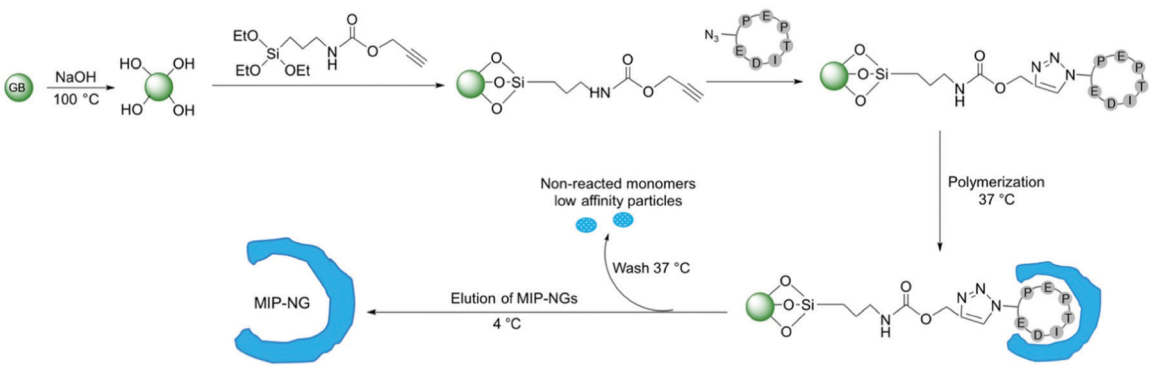

Fig. 3 Schematic representation of the solid-phase synthesis of MIP. The cyclic peptide template bearing an azide moiety is immobilized on alkyne-GBs *via* click chemistry, followed by polymerization at 37 °C to form thermoresponsive MIP-NGs. After washing away the non-reacted monomers and low affinity polymers, the MIP-NGs are released from the GBs by decreasing the temperature to 4 °C.

monomer, 4-acrylamidophenyl(amino)-methanimium acetate (AB) was employed to form a salt bridge with the carboxylic group of aspartic acid. *N*,*N*′-methylenebis(acrylamide) (BIS) was used as cross-linker and free radical polymerization was carried out at 37 °C in sodium phosphate buffer pH 7.0. At this temperature, the polymers are formed in the collapsed state, encapsulating the immobilized peptide. After washing away the low-affinity nanogels and the unreacted monomers, the polymers that presented high affinity to the peptide were eluted at 4 °C, below the lower critical solution temperature of *p*(NIPAM) (LCST, ~32 °C), where the NGs swell and are detached from the column. The yield of polymerization of the MIP-NGs was 0.25 ± 0.03 mg g^{-1} GBs (n = 3), comparable to previous reports.[25,27,29]

Physicochemical characterization and binding properties of MIP-NGs

The hydrodynamic size of MIP-NGs was analyzed by dynamic light scattering (DLS) and found to be 47.7 ± 2.5 nm, PDI 0.32 ± 0.05 and a zeta potential of +9.8 mV (Fig. S1A and B, ESI†). Transmission electron microscope (TEM) images showed that the MIP-NGs were monodisperse (Fig. S1C, ESI†) and confirmed the size determined by DLS. The recognition of the peptide epitope by the MIP was evaluated at 37 °C by equilibrium binding assays with the fluorescently labelled template (coupled to fluorescein dibenzocyclooctyne, FAM DBCO) *via* a copper-free click chemistry reaction (Fig. S2A, ESI†). This fluorophore was chosen for its bulky DBCO, to favor the accomodation of only the peptide in the MIP binding cavity. The fluorescent peptide was purified by preparative HPLC and its purity analyzed by electrospray ionization high-resolution mass spectrometry (Fig. S2B, ESI†). The concentration of the pure fluorescent peptide was found to be 22.4 ± 3.5 μM (Fig. S3, ESI†). Equilibrium binding experiments showed that the binding of the MIP-NGs to the fluorescent peptide was specific as no binding was observed with the control polymer, a MIP with the same chemical composition synthesized with the peptide DWVIPPI (Fig. 4). These results confirmed the presence of specific imprinted sites at the surface of the nanogels.

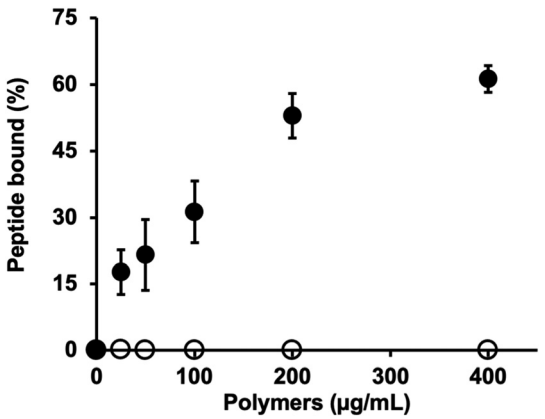

Fig. 4 Equilibrium binding isotherms of 10 nM of fluorescent template peptide to MIP-NGs (full circles) and control polymer (empty circles) at 37 °C in sodium phosphate buffer pH 7.0 (n = 3, mean ± s.e.m.).

Table 1 IC_{50} values of the MIP-NGs with various competitors, as determined by competitive binding assays with the fluorescently labelled template peptide epitope

Competitor	Molecular weight[a] (Da)	Isoelectric point[a]	IC_{50} (nM)
Template peptide CAHAVDINGC-K(N_3)	1153.49	4.98	300
Short cyclic peptide CHAVDINC-K(N_3)	1025.44	4.98	36 400
HAVDI linear peptide	553.29	4.98	>100 000
DWVIPPI linear peptide	838.46	3.11	No binding
N-cadherin	62 910	4.7	25
E-cadherin	60 586	4.28	41
P-cadherin	87 400	4.55	200

[a] Theoretical molecular weight and isoelectric point.

Selectivity was evaluated by competitive binding assays in the presence of the native template peptide CAHAVDINGC-K(N_3), a shorter cyclic peptide CHAVDINC-K(N_3) containing the same motif, linear peptides HAVDI and DWVIPPI, as well as recombinant E-, N- and P-cadherins (Fig. S4, ESI†). Increasing concentrations of the peptides or proteins competed with a fixed amount of the fluorescently labelled peptide for binding to the MIP-NGs. The IC_{50} values (concentration of inhibitor required to displace 50% of the fluorescent peptide from the MIP) are shown in Table 1. IC_{50} values of 300 nM and 25 nM were found for the template peptide and N-cadherin respectively, indicating the excellent recognition of the MIP-NGs for their target. The higher affinity for the protein, as compared to the peptide epitope, may be due to the contribution of the protein surface in contact with the MIP-NGs (displacement of solvent molecules, conformational rearrangements of main and side chain atoms), which leads to improved complementarity and stability. MIP-NGs' binding to the shorter version of the cyclic peptide was negligible, probably due to the fact that the different lengths of the peptides lead to different curvatures and flexibility. Thus, the shorter peptide has less contact area with the cavity in the polymer. It is interesting to note that the MIP-NGs have almost no affinity for the linear HAVDI peptide. A reduced interaction has been previously observed between a MIP directed against a cyclic epitope, and the linear version of the epitope.[31] No interaction with the peptide DWVIPPI was observed. E-cadherin, containing the sequence SHAVSSNG and P-cadherin, with the sequence GHAVSENG, presented IC_{50} values of 41 and 200 nM, respectively, implying that the MIP-NGs also recognized E-cadherin and P-cadherin to a certain extent, but less well as compared to the target N-cadherin. Globally, the MIP-NGs appear to bind the proteins somewhat more strongly than the template epitope peptide, a phenomenon that we have often observed with other examples (unpublished data), and that can be attributed to the induced-fit and surface effects mentioned above.

Despite the MIP having 60% cross-reactivity with E-cadherin, this synthetic receptor represents a superior antagonist of N-cadherin as compared to the different peptides reported in the literature.[13] The simplest cyclic peptide *N*-Ac-CHAVC-NH_2 inhibited N-cadherin with

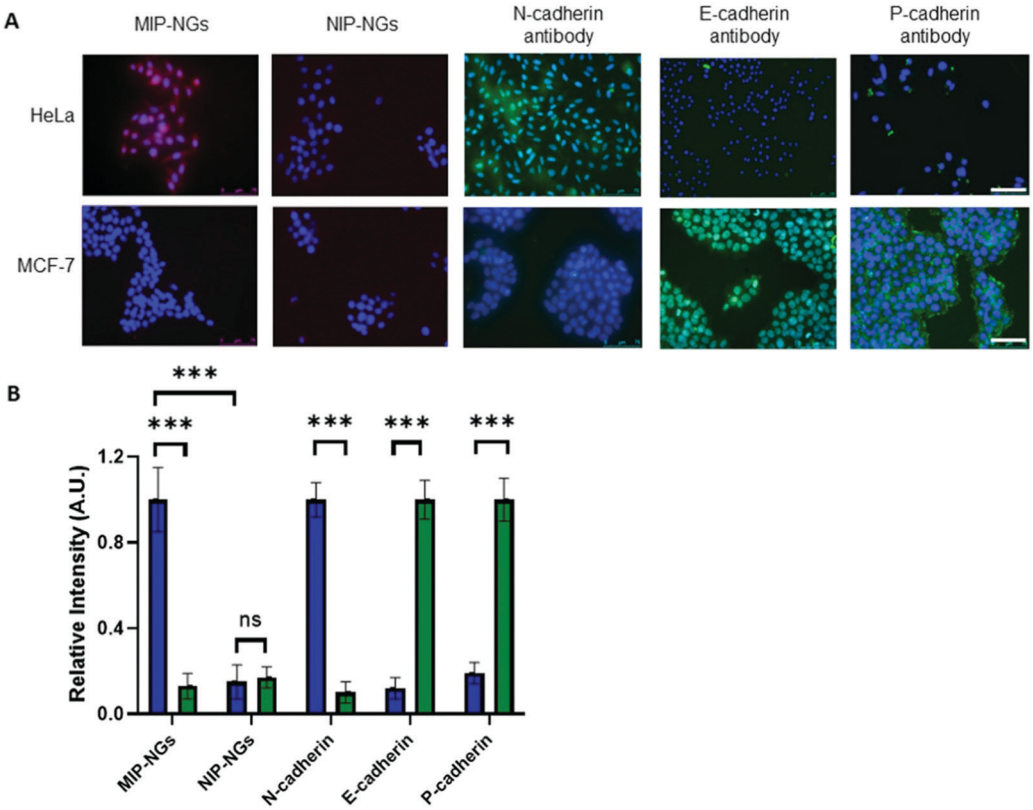

Fig. 5 (A) Epifluorescence micrographs of HeLa (overexpressing N-cadherin) and MCF-7 cells (overexpressing E- and P-cadherin), stained with rhodamine MIP-NGs (red) or rhodamine NIP-NGs (red) or anti N-, E- and P-cadherin antibodies (green). Nuclei stained with Hoechst (blue). Scale bar: 75 μm. (B) Corresponding relative fluorescence intensity of HeLa (blue) and MCF-7 (green) cells after imaging with MIP-NGs or NIP-NGs or immunostaining with N-, E- or P-cadherin antibodies. Data are expressed as mean ± SEM, statistical analysis was performed using Student's test (***$p < 0.001$), ns: not significant.

an IC_{50} of 0.323 ± 0.020 mM. When the cyclic HAV peptide was turned into an N-cadherin peptide by incorporating flanking amino acids specific to N-cadherin, the antagonistic properties of the peptides were increased. For instance, the cyclic peptides *N*-Ac-CHAVDC-NH_2, *N*-Ac-CHAVDIC-NH_2 and *N*-Ac-CAHAVDIC-NH_2 presented IC_{50} values of 0.114 ± 0.006 mM, 0.065 ± 0.005 mM and 0.210 mM respectively. Interestingly, when the HAVDI peptide was tested as a linear peptide (*N*-Ac-HAVDI-NH_2), a 7-fold reduction in the activity was observed (IC_{50} of 0.44 ± 0.014 mM) as compared to the cyclic analogue. These results imply that the MIP is a better antagonist than the peptides by almost three orders of magnitude.

Recognition of cadherins on cells

Since the MIP-NGs seem to recognize free N-cadherin (and to a lesser extent E-cadherin) protein in solution, the next step was to verify whether they could recognize these proteins at the cell surface. Fluorescent MIP-NGs were synthesized by incorporating polymerizable rhodamine B in the pre-polymerization mixture, as previously reported.[21,29] Their hydrodynamic diameter was measured by DLS and found to be 44 ± 2.1 nm, with a polydispersity index of 0.29 ± 0.04 ($n = 3$). The MIP-NGs were then applied to two human cancer cell lines with different cadherin expression profiles: HeLa (expressing N-cadherin) and MCF-7 (breast cancer expressing E- and P-cadherins). The cadherin profile in the two cell lines was prior verified by staining with anti E-, N- and P-cadherin antibodies (Fig. 5A and B). MIP-NGs were found to bind to the surface of HeLa cells, indicating that their preferential target is N-cadherin. While in free solution, the MIP-NGs seemed to bind (to a lesser extent also E-cadherin), no evidence of staining by rhodamine MIP-NGs was observed on fixed MCF-7 cells. This result indicates that the selected epitope CAHAVDINGCK(N_3) generated a MIP-NG selective for N-cadherin, although we have no explanation for this improved specificity over the solution experiment; the only difference being that in solution we have used recombinant proteins. No staining on L929 mouse fibroblasts, an additional control cell line, which does not express endogeneous cadherins was observed either (Fig. S5, ESI†).[32] No staining was obtained with the non-imprinted control nanogels (NIP-NGs).

Inhibition of cell aggregation by MIP-NGs

Cell aggregation assays have become a useful tool to study cadherin-dependent adhesion, given that cell aggregation is the net result of cell-cell adhesion.[7] HeLa and MCF-7 cells were suspended in agar-coated microtiter wells to exclude cell-substrate adhesion while allowing cell-cell interactions to occur. Prior to incubation with cells, MIP-NGs were checked

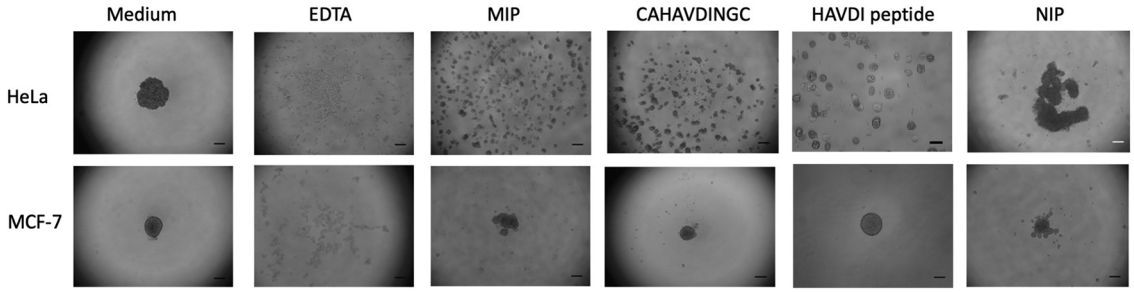

Fig. 6 Effect on HeLa and MCF-7 (200 000 cells per mL) cell aggregation when incubated with 4 mM EDTA, 20 μg mL^{-1} MIP, 100 nM template peptide, 100 nM HAVDI linear peptide and 20 μg mL^{-1} NIP, in growth medium. Scale bar: 250 μm.

for their non-cytotoxicity using the MTT assay (Fig. S6, ESI†). Cells were incubated in the presence of either MIP, NIP (a control polymer synthesized against azide-functionalized GBs) or the cyclic template CAHAVDINGC-K(N_3) or the linear HAVDI peptide for 24 h; the formation of cell aggregates was evaluated under an inverted microscope. Cells incubated with only medium were taken as reference, and cells incubated with ethylenediaminetetraacetic acid (EDTA) served as positive control (EDTA chelates Ca^{2+} ions and cell-cell aggregation is abrogated).

As illustrated in Fig. 6, HeLa and MCF-7 cells incubated in only growth medium showed one tight aggregate. On the contrary, no cell cluster was observed in the presence of EDTA, suggesting that cell aggregation was disrupted. For HeLa cells, addition of MIP and the cyclic peptide CAHAVDINGC resulted in numerous dispersed aggregates, indicating their ability to prevent cell-cell adhesion. Inhibition of cell aggregation by MIP-NGs was concentration-dependent (Fig. S7, ESI†). Slightly smaller aggregates were observed with the MIP than with the peptide, indicating the better antagonist properties of the MIP to N-cadherin than the cyclic peptide. On the other hand, the HAVDI linear peptide when compared with cyclic peptide CAHAVDINGC, was not very effective in cell disruption. In the case of MCF-7 cells which lack N-cadherin but which contain E-cadherin, the MIP caused a very slight dispersion in cell aggregation. For both cell lines, the NIP does not really affect cell aggregation, since the main cell cluster was preserved. These observations suggest that MIPs render cells incapable of establishing cell-cell adhesion by binding to the adhesive motif, HAVDI of N-cadherin. The specificity of the inhibition by the MIP was confirmed by the lower effect produced in MCF-7, a cell line lacking N-cadherin, and by the lower impact observed with the NIP.

Inhibition of cancer cell invasion by MIP-NGs

Matrigel® invasion assay[33] was employed to assess the invasion propensity of HeLa cells in the presence of MIP-NGs. Matrigel acts as a reconstituted basement membrane and prevents non-invasive cells from passing across, whereas invasive cells enzymatically degrade the Matrigel membrane and invade through its pores. HeLa cells (25 000) were seeded onto a Matrigel-coated insert with or without MIP-NGs (30 μg mL^{-1}) and incubated for 24 h. Cells that migrated to the lower side of the membrane were stained and evaluated by epifluorescence microscopy. Fig. 7 shows that cells seeded with MIP-NGs showed a significant decrease in their invasive capacity as

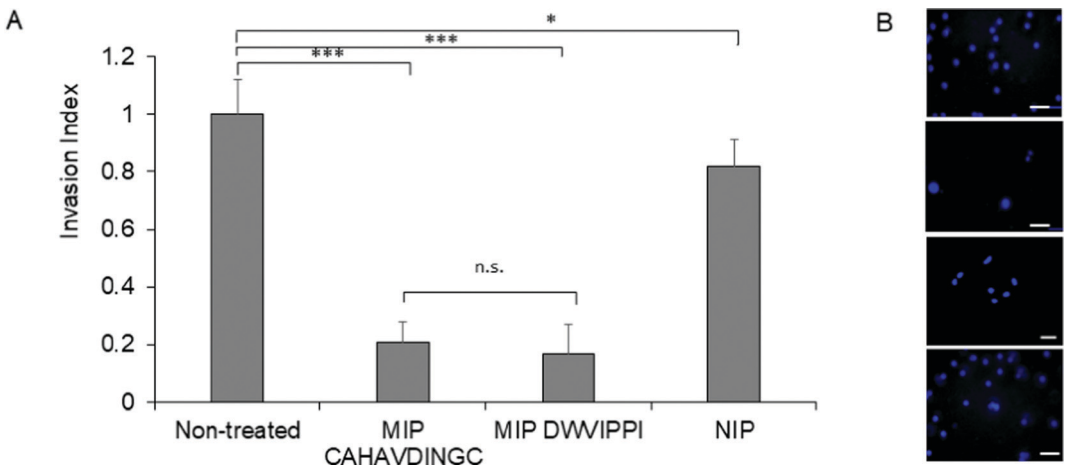

Fig. 7 Fig. 7. (A) Invasion index representing the extent of HeLa cells invasion in the presence of MIP or NIP, as studied by Matrigel Invasion assay. As a positive control, MIP targeting DWVIPPI[21] was tested in parallel. Mean values are significantly different at 95% confidence (*$p < 0.05$, ***$p < 0.001$, n.s, not significant, Student's t-test, mean ± s.e.m.). (B) Epifluorescence micrographs of HeLa cells that invaded to the lower side of the Matrigel membrane. Cells were stained with Hoechst. From top to bottom: untreated cells, cells treated with MIP (CAHAVDINGC), MIP (DWVIPPI) and NIP. Scale bar: 25 μm.

compared to non-treated cells and NIPs. The MIP-NGs synthesized with CAHAVDINGC (IC_{50}: 25 nM) was as efficient as the MIP-NGs synthesized with DWVIPPI[21] (IC_{50}: 20 nM) for blocking cancer invasion *in vitro*.

Overall, these results indicate that MIPs can exhibit a biological activity by modulating cadherin activity; this can lead to new approaches to treat diseases associated with dysfunctional cadherin mechanisms.

Conclusion

In a precedent paper,[21] we synthesized a MIP-NG targeting the first seven amino acids of the N-terminal part of E- and N-cadherins, which encompasses Trp2, an amino acid responsible for cell adhesion. The inhibitory potency of this MIP towards cell-cell adhesion in cell aggregation assays proved to be remarkably higher than that of a commercially available monoclonal antibody, known to inhibit cadherin adhesion. Importantly, this MIP could inhibit cancer cells invasion and disrupt three-dimensional tumour spheroids, highlighting the promising therapeutic value of MIPs in cancer treatment. In the present work, we hypothesized that it should also be possible to block the entrance of the acceptor domain of Trp2, a hydrophobic pocket lined by the sequence HAV. Thus a MIP-NG templated with a cyclic peptide CAHAVDINGC was synthesized. It has a high affinity and selectivity for N-cadherin over E and P-cadherins. This MIP-NG was very effective in abrogating cancer cell adhesion and invasion, confirming the high potential of MIPs as a therapeutic drug. These findings are in line with recent literature data where MIPs imprinted against HER2 glycans were shown to inhibit cell proliferation and reduce cancer volume *in vivo*.[34] We believe that MIPs can successfully contribute to the establishment of a novel therapeutic platform in cancer treatment.[35–37]

Experimental section

Materials and methods

All chemicals and solvents were of analytical grade and purchased from VWR International (Fontenay sous Bois, France) or Sigma-Aldrich (St Quentin Fallavier, France), unless otherwise stated. (*O*-(Propargyloxy)-*N*-(triethoxysilylpropyl)urethane was purchased from Abcr GmbH, Germany. Peptides (purity >95%) were custom-synthesizsed by GL Biochem (Shanghai, China). Recombinant human E-cadherin (purity ≥90%, expressed in *E. coli*) was obtained from Sigma-Aldrich. Recombinant human N-cadherin (purity >90%, expressed in Sf9 Baculovirus cells) was bought from Interchim (Montluçon, France). Recombinant human P-cadherin Fc Chimera Protein (purity >90%) was purchased from R&D Systems (Lille, France). FAM DBCO, 6-isomer and tris(3-hydroxypropyltriazolylmethyl)amine (THPTA) were purchased from Interchim. HeLa and MCF-7 were obtained from Cell Lines Service (Eppelheim, Germany). Media, reagents and consumables for cell culture were from Thermo Fisher Scientific (Illkirch, France). Glass beads of diameter 0.1 mm and microscope slides for cell samples were bought from Roth Sochiel E.U.R.L. (Lauterbourg, France). Buffers were prepared with Milli-Q water, purified using a Milli-Q system (Millipore, Molsheim, France). Fluorescence measurements were done on a FluoroLog-3 spectrofluorimeter (Horiba Jobin Yvon, Longjumeau, France). Transmission electron microscopy images were recorded on a a JEOL JEM-2100F instrument (Japan). Cell aggregation was evaluated under a Leica inverted microscope equipped with camera (Nanterre, France).

Synthesis of MIP-NGs

Peptide immobilization on glass beads. Glass beads (GBs) were first activated by boiling in 4 M NaOH (100 g of GBs in 100 mL of NaOH), for 10 min. The activated GBs were then washed with water and acetone and then dried in an oven at 50 °C. Alkyne functionalization was done on 50 g activated GBs by incubation in 100 mL *O*-(propargyloxy)-*N*-(triethoxysilylpropyl)urethane 5% (v/v) in dimethyl formamide (DMF), in an oil-bath at 90 °C for 17 h. The alkyne GBs were washed with DMF and acetone and dried in an oven at 50 °C. Immobilization of the peptide template CAHAVDINGC-K(N_3) onto the solid phase was performed *via* CuAAC reaction. In a Petri dish (12 cm diameter), 20 g azide GBs were incubated with 6.4 μmol peptide, 6.4 μmol of $CuSO_4.5H_2O$, 32 μmol of THPTA and 50.4 μmol of sodium ascorbate in 25 mM sodium phosphate buffer, pH 7.0 (buffer A), final volume 12 mL. After 1 h incubation, the GBs were washed with buffer A and water, and used immediately. The ratio among the reagents was 1 : 1 : 5 : 8 (alkyne peptide : $CuSO_4$: THPTA : sodium ascorbate).[29]

Solid-phase synthesis of MIP

Solid-phase synthesis was carried out in a glass column equipped with a thermostated jacket (XK 26/20). The solvents were pumped through the column using a peristaltic pump at a flow rate of 2.5 mL min^{-1}. The column was packed with 20 g peptide GBs and equilibrated with 100 mL buffer A. Then, 20 mL of buffer A containing 4-acrylamidophenyl(amino)-methaniminium acetate (AB, benzamidine-based monomer) (12.4 mg, 0.05 mmol, 5 mol%) was percolated through the column. The flow-through was collected and passed through the column again for 1 h to favour the AB interaction with the -COOH moieties of the peptide. The polymerization mixture was prepared by mixing the rest of the monomers, *N*-isopropylacrylamide (NIPAM) (92.8 mg, 0.82 mmol, 82 mol%), *N*-*tert*-butylacrylamide (TBAM) (10.2 mg dissolved in 1 mL ethanol, 0.08 mmol, 8 mol%) and *N*,*N*′-methylenebis(acrylamide) (BIS) (7.7 mg, 0.05 mmol, 5 mol%) in 25 mL with buffer A so that the total monomer concentration is 0.5% (w/w). The solution was purged with nitrogen for 30 min. Afterwards, the initiation couple composed of potassium persulfate (KPS) (8.5 mg in 500 μL buffer A) and *N*,*N*,*N*,*N*′-tetramethylethylendiamine (TEMED) (63 μL of 10 μL of TEMED in 990 μL buffer A) was added to the reaction mixture. The amount of KPS was 3% (mol/mol) with respect to polymerizable double bonds, and 7.5/1 was the molar ratio for KPS/TEMED. The polymerization mixture was percolated through the reactor, and the temperature was set at 37 °C for 17 h. After polymerization, the column was washed with 50 mL buffer A at 37 °C, and the column was cooled down at 4 °C for 1 h. MIP was

eluted by fractions of 6 mL (twice) with water and constituted the working stock solution. The hydrodynamic diameter of MIPs, analyzed by dynamic light scattering (DLS), and their zeta potential were determined by using a Malvern Zetasizer Nano ZS. The concentration of the MIPs was calculated with a 3 mL aliquot of MIP, which was lyophilized and weighed.

Evaluation of the binding properties of MIP-NGs

Fluorescence labelling of template peptide. Binding properties were evaluated by using the fluorescently-labelled peptide template. For its synthesis, a copper-free click chemistry reaction was performed by mixing 500 μL of a 1 mM of peptide CAHAVDINGC-K(N_3) and 1 mM FAM DBCO, 6-isomer in a final volume of 1 mL water. After 3 h, the peptide clicked with FAM (expected mass: 1829.7 g mol^{-1}) was purified by semi-preparative HPLC, using a Phenomenex Luna® C18(2) (250 × 10 mm, 5 μm, 100 Å) column connected to an Agilent Infinity II 1260 HPLC apparatus. The solvent system was A: 0.1% formic acid in H_2O and B: acetonitrile. The gradient program began and stayed at 5% B during 5 min, then ramped to 30% B at 20 min, increased to 95% B in 15 min, held at 95% during 10 min, returned to the initial conditions and kept constant for 3 min. The flow-rate was 7 mL min^{-1}. Detection was done at 280 nm. The fraction collector was set to collect fractions between 24 and 26 min with a threshold of 20 mAu to 4000 mAu, up slope of 50 mAu s^{-1}. The fractions were analyzed by HPLC-UV coupled to high resolution mass spectrometry (LC-HRMS). LC-HRMS was performed on an HPLC Agilent 1290 with DAD connected to Agilent Q-TOF 6538 with an electrospray ion source (ESI). HPLC was carried out on a Thermo Hypercyl GOLD C18 (100 × 2.1 mm, 1.9 μm) column connected to an Agilent Infinity 1290 HPLC. The solvent system was A: 0.1% formic acid in H_2O and B: acetonitrile. The gradient program began and stayed at 5% B during 1 min, then ramped to 30% B at 5 min and increased to 95% B in 5 min, held à 95% during 2 min, returned to the initial conditions and kept constant for 1 min. The flow-rate was 0.4 mL min^{-1}. All compounds were measured in ESI^+ mode and externally calibrated. The ESI gas temperature was 350 °C, Vcap +3800 V, drying gas 12 L min^{-1} and nebuliser 35 psig. Fragmentor was set à 180 V. HRMS spectrum was registered at 3 Hz in the mass range of 100 to 3000 m/z with internal calibration. The purity of the fluorescent cyclic peptide was ≈99.8%.

Determination of FAM-labelled peptide concentration. A fluorescence calibration curve (λ_{ex} 490 nm, λ_{em} 500–560 nm, slit 1 nm) was first generated with increasing concentrations of FAM DBCO (0.1–5 μM) in buffer A. For the quantification of the fluorescent peptide, the peptide solution was diluted 25 and 50-fold in buffer A so as to fall within the calibration curve of the underivatized dye. The concentration was found to be 22.4 ± 3.5 μM. Afterwards, a calibration curve was generated with the FAM-peptide at nanomolar concentrations (490 nm/500–560 nm, slit 4 nm). 10 nM was selected for binding tests with the polymer nanogels.

Equilibrium binding studies. From an initial stock solution of 0.5 mg mL^{-1} MIP, different concentrations (25–400 μg mL^{-1}) were pipetted in separate 2 mL polypropylene microcentrifuge tubes. After addition of 10 pmol (50 μL of 200 nM) of fluorescent peptide (fluorescently labelled with FAM), the final volume was completed to 1 mL with buffer A and the mixture was incubated overnight at 37 °C on a tube rotator. The samples were centrifuged at 30 000g for 1 h at 40 °C and the fluorescence intensity of a 700 μL aliquot was measured (λ_{ex}: 490 nm/λ_{em}: 515 nm, slit 4 nm) to determine the amount of free peptide. The amount of peptide bound to the polymer was calculated by subtracting the unbound analyte from the total peptide added to the mixture determined from the blank samples.

Selectivity studies. The peptides CAHAVDINGC-K(N_3) (cyclic native), CHAVDINC-K(N_3) (shorter cyclic), HAVDI (linear) and DWVIPPI (linear, the N-terminal adhesive motif) were added at varying concentrations from (0.1 nM-100 μM) to compete with 10 nM FAM-peptide in 1 mL buffer A containing 200 μg mL^{-1} of MIP. The recombinant human proteins N-, E- and P-cadherins were added from 0.1–100 nM. Fluorescence measurements were done as mentioned above. IC_{50} values were determined by fitting the data to a sigmoidal dose-response curve.

Application of MIP-NGs to cells

Cell culture. HeLa and MCF-7 were cultured in Dulbecco's Modified Eagle Medium (DMEM)-high glucose with 10% fetal bovine serum (FBS) and 1% penicillin/streptomycin medium in a 75 cm^2 flask at 37 °C, 5% CO_2 and 100% humidity, referred as full medium. Cells were passaged at 80% confluency using 0.25% trypsin/EDTA in PBS, prior washing with 0.05% EDTA in PBS.

Cell viability assays. Cell viability in the presence of MIP-NGs was determined by the MTT assay, which assesses the metabolic activity of living cells. MCF-7 and HeLa cells were grown in each well of a 96-well plate (15 000 cells per well). After 24 h, cells were incubated with MIP-NGs (5–250 μg mL^{-1}) for 24 h in cell culture medium. Dissolution of the crystals of MTT was achieved by DMSO and Sorensen's buffer. Cell viability was determined by dividing the absorbance obtained for treated cells by that of the untreated controls. Cell treated with 1% Triton X-100 served as positive control of cytotoxicity.

Cell fixation and bioimaging

With monoclonal antibodies. Immunostaining with E-cadherin antibody (clone DECMA-1), N-cadherin antibody (clone 5D5) and P-cadherin antibody (clone 104805) was performed to confirm the presence of the cadherins on MCF-7 and HeLa cells. Staining with antibodies was done according to the instructions given by the manufacturer. 100 μL of cells (1 × 10^5 cells) was cultured on round glass cover slips (diameter 12 mm) contained in 12-well plates. After 3 h of incubation, 2 mL medium was added to the wells, and cells were left to grow to confluency for 24-48 h. Cells were then washed with 1 mL PBS (3 times) and fixed with 4% paraformaldehyde in PBS for 15 min. After fixation, cells were washed with PBS, followed by a blocking step with 5% bovine serum albumin (BSA) in PBS for 1 h at room temperature and washing with PBS. For E-cadherin staining, the cell membrane was permeabilized with

0.1% Triton X-100 for 15 min, blocked with BSA and labelled with the primary antibody in 0.1% BSA in PBS at 4 °C overnight, followed by incubation with anti-Rat IgG secondary antibody-FITC at a dilution of 1 : 400 in 1% BSA in PBS for 30 min. For P-cadherin staining, the cell membrane was permeabilized and the cells incubated with primary antibody in 1% BSA in PBS for 3 h, followed by incubation with Alexa Fluor 488 anti-Mouse IgG secondary antibody at a dilution of 1 : 400 in 1% BSA in PBS for 30 min. For N-cadherin staining, Alexa Fluor 488 anti-Mouse IgG was also used as secondary antibody and for all cells, the nuclei were stained with Hoechst at a dilution of 1 : 2000 in PBS at room temperature for 10 min. Cells were washed with PBS, mounted on a microscope slide with 5 μL mounting medium (0.5 mL water, 0.5 mL 1 M Tris-HCl buffer pH 8.0 and 9 mL glycerol) and analyzed with a Leica DMI 6000B epifluorescence microscope. Each sample was prepared in duplicate.

With MIP or NIP nanogels. Cells were grown and fixed as described for the antibodies. Staining was done with 50 μg mL^{-1} rhodamine-labelled MIP-NGs or NIP-NGs in buffer at 37 °C for 90 min. After washing with buffer (twice) and 0.1% Tween 20 in PBS (twice), cell nucleus was stained by incubation with Hoechst in PBS at a dilution of 1 : 2000 at room temperature for 10 min. Cells were washed with PBS, mounted on a microscope slide with 5 μL mounting medium (0.5 mL water, 0.5 mL 1 M Tris–HCl buffer pH 8.0 and 9 mL glycerol) and analyzed by fluorescence microscopy. Epifluorescence microscopy images were recorded with a Leica DMI 6000B (Germany) microscope. Each sample was prepared in triplicate and the fluorescence intensities were measured with ImageJ. Three images per sample with 40x magnification were analyzed, by measuring the relative fluorescence of 10 cells per image.

Cell aggregation studies. Cell aggregation agar assays were performed as previously reported.[21] Briefly, 100 mg agar in 15 mL PBS was sterilized and 50 μL was pipetted into each well of a 96-well plate, after which the plate was placed at 4 °C on a horizontal surface for 1 h to allow the agar to solidify. Afterwards, 100 μL of a suspension of HeLa or MCF-7 cells in full medium (200 000 cells per mL) was added to the agar-coated wells, followed by the addition of 100 μL of the test product in full medium. The polymers were tested at 20 μg mL^{-1}, EDTA at 4 mM, the cyclic peptide CAHAVDINGC-K(N_3) at 100 nM. Cells incubated with only medium were taken as control. The well-plates were incubated at 37 °C, 5% CO_2 and 100% humidity under horizontal stirring. Cell aggregation was evaluated at 24 h after seeding cells, under an inverted microscope equipped with a camera using a 4x objective and bright contrast.

Inhibition of HeLa cell invasion through Matrigel® by MIP-NGs. Tumour cell invasion assay through Matrigel was performed on Corning® BioCoat™ Matrigel® Invasion Chambers, according to the manufacturer's instructions. HeLa cells (25 000) suspended in DMEM medium, in the presence or absence of 30 μg mL^{-1} MIP-NGs or NIP-NGs, were seeded on Matrigel-coated inserts, whereas the lower compartment contained DMEM medium supplemented with 10% FBS as chemoattractant. After 24 h incubation at 37 °C, 5% CO_2 and 100% humidity, the upper surface of the insert was cleared from non-migratory cells with a cotton swab and washed with PBS. The remaining (invasive) HeLa cells that attached to the lower surface of the filter were fixed with cold methanol, stained with Hoechst (at a dilution of 1 : 2000 in PBS for 10 min) and analyzed with an epifluorescence microscope at 63x of magnification, using the filter A4. Invasive cells were quantified as the number of migrated cells per microscopic field, 10 fields per assay from two independent repetitions. Invasion index was calculated as the ratio between the number of invasive HeLa cells treated with MIP-NGs or NIP-NGs and the number of invasive HeLa (without polymer).

Conflicts of interest

There are no conflicts to declare.

Acknowledgements

P. X. M. R. thanks the Mexican National Council for Science and Technology (CONACYT) and the Instituto para el Desarrollo de la Sociedad del Conocimiento del Estado de Aguascalientes (IDSCEA), for PhD scholarship. A. M. thanks CONACYT and the Instituto de Innovación y Transferencia de Tecnología de Nuevo Leon for PhD scholarship. E. M. thanks the Erasmus+ program for financial support. The authors acknowledge financial support from the Region of Picardy and the European Union (co-funding of equipment under CPER 2007–2020 and project POLYSENSE). B. T. S. B. acknowledges COST Action CA18013 ''Innovation with Glycans: new frontiers from synthesis to new biological targets''. K. H. acknowledges financial support from Institut Universitaire de France.

References

1 C. Yoshida-Noro, N. Suzuki and M. Takeichi, *Dev. Biol.*, 1984, **101**, 19–27.
2 T. J. Boggon, J. Murray, S. Chappuis-Flament, E. Wong, B. M. Gumbiner and L. Shapiro, *Science*, 2002, **296**, 1308–1313.
3 K. M. Mrozik, O. W. Blaschuk, C. M. Cheong, A. C.-W. Zannettino and K. Vandyke, *BMC Cancer*, 2018, **18**, 939.
4 M. Takeichi, *Curr. Opin. Cell Biol.*, 1993, **5**, 806–811.
5 W. Yu, L. Yang, T. Li and Y. Zhang, *Front. Oncol.*, 2019, **9**, 989.
6 V. Padmanaban, I. Krol, Y. Suhail, B. M. Szczerba, N. Aceto, J. S. Bader and A. J. Ewald, *Nature*, 2019, **573**, 439–444.
7 K. Tamura, W. S. Shan, W. A. Hendrickson, D. R. Colman and L. Shapiro, *Neuron*, 1998, **20**, 1153–1163.
8 S. C. Newton, O. W. Blaschuk and C. F. Millette, *Dev. Dyn.*, 1993, **197**, 1–13.
9 H. Tanaka, E. Kono, C. P. Tran, H. Miyazaki, J. Yamashiro, T. Shimomura, L. Fazli, R. Wada, J. Huang, R. L. Vessella, J. An, S. Horvath, M. Gleave, M. B. Rettig, Z. A. Wainberg and R. E. Reiter, *Nat. Med.*, 2010, **16**, 1414–1421.

10 O. W. Blaschuk, *Cell Tissue Res.*, 2012, **348**, 309–313.
11 C. C. Zhang, Z. Yan, Q. Zhang, K. Kuszpit, K. Zasadny, M. Qiu, C. L. Painter, A. Wong, E. Kraynov, M. E. Arango, P. P. Mehta, L. Popoff, G. F. Casperson, G. Los, S. Bender, K. Anderes, J. G. Christensen and T. VanArsdale, *Clin. Cancer Res.*, 2010, **16**, 5177–5188.
12 S. M. Brouxhon, S. Kyrkanides, X. Teng, V. Raja, M. K. O'Banion, R. Clarke, S. Byers, A. Silberfeld, C. Tornos and L. Ma, *Clin. Cancer Res.*, 2013, **19**, 3234–3246.
13 E. Williams, G. Williams, B. J. Gour, O. W. Blaschuk and P. Doherty, *J. Biol. Chem.*, 2000, **275**, 4007–4012.
14 S. M. Burden-Gulley, T. J. Gates, S. E.-L. Craig, S. F. Lou and S. A. Oblander, *Peptides*, 2009, **30**, 2380–2387.
15 G. M. Beasley, J. C. Riboh, C. K. Augustine, J. S. Zager, S. N. Hochwald, S. R. Grobmyer, B. Peterson, R. Royal, M. I. Ross and D. S. Tyler, *J. Clin. Oncol.*, 2011, **29**, 1210–1215.
16 R. M. Mege, D. Goudou, C. Diaz, M. Nicolet, L. Garcia, G. Geraud and F. Rieger, *J. Cell Sci.*, 1992, **103**, 897–906.
17 B. D. Cosgrove, K. L. Mui, T. P. Driscoll, S. R. Caliari, K. D. Mehta, R. K. Assoian, J. A. Burdick and R. L. Mauck, *Nat. Mater.*, 2016, **15**, 1297–1306.
18 R. Arshady and K. Mosbach, *Makromol. Chem.*, 1981, **182**, 687–692.
19 G. Wulff, A. Sarhan and K. Zabrocki, *Tetrahedron Lett.*, 1973, **14**, 4329–4332.
20 K. Haupt, A. V. Linares, M. Bompart and B. Tse Sum Bui, *Top. Curr. Chem.*, 2012, **325**, 1–28.
21 P. X. Medina Rangel, E. Moroni, F. Merlier, L. A. Gheber, R. Vago, B. Tse Sum Bui and K. Haupt, *Angew. Chem., Int. Ed.*, 2020, **59**, 2816–2822.
22 K. Haupt, P. X. Medina Rangel and B. Tse Sum Bui, *Chem. Rev.*, 2020, **120**, 9554–9582.
23 L. O'Driscoll, *N. Engl. J. Med.*, 2020, **383**(9), 871–873.
24 J. Xu, F. Merlier, B. Avalle, V. Vieillard, P. Debré, K. Haupt and B. Tse Sum Bui, *ACS Appl. Mater. Interfaces*, 2019, **11**, 9824–9831.
25 A. Mier, I. Maffucci, F. Merlier, E. Prost, V. Montagna, G. U. Ruiz-Esparza, J. V. Bonventre, P. K. Dhal, B. Tse Sum Bui, P. Sakhaii and K. Haupt, *Angew. Chem., Int. Ed.*, 2021, **60**, 20849–20857.
26 S. Ambrosini, S. Beyazit, K. Haupt and B. Tse Sum Bui, *Chem. Commun.*, 2013, **49**, 6746–6748.
27 J. Xu, S. Ambrosini, E. Tamahkar, C. Rossi, K. Haupt and B. Tse Sum Bui, *Biomacromolecules*, 2016, **17**, 345–353.
28 A. Poma, A. Guerreiro, M. J. Whitcombe, E. V. Piletska, A. P.-F. Turner and S. A. Piletsky, *Adv. Funct. Mater.*, 2013, **23**, 2821–2827.
29 P. X. Medina Rangel, S. Laclef, J. Xu, M. Panagiotopoulou, J. Kovensky, B. Tse Sum Bui and K. Haupt, *Sci. Rep.*, 2019, 9, 3923.
30 R. A. Reid and J. J. Hemperly, *Nucleic Acids Res.*, 1990, **18**, 5896.
31 L. Cenci, G. Guella, E. Andreetto, E. Ambrosi, A. Anesi and A. M. Bossi, *Nanoscale*, 2016, **8**, 15665–15670.
32 S. V. Litvinov, M. Balzar, M. J. Winter, H. A.-M. Bakker, I. H. Briaire-de Bruijin, F. Prins, G. J. Fleuren and S. O. Warnaar, *J. Cell Biol.*, 1997, **139**, 1337–1348.
33 A. S. Ribeiro, A. Albergaria, B. Sousa, A. L. Correia, M. Bracke, R. Seruca, F. C. Schmitt and J. Paredes, *Oncogene*, 2010, **29**, 392–402.
34 Y. Dong, W. Li, Z. Gu, R. Xing, Y. Ma, Q. Zhang and Z. Liu, *Angew. Chem., Int. Ed.*, 2019, **58**, 10621–10625.
35 T. Takeuchi, K. Mori, H. Sunayama, E. Takano, Y. Kitayama, T. Shimizu, Y. Hirose, S. Inubushi, R. Sasaki and H. Tanino, *J. Am. Chem. Soc.*, 2020, **142**, 6617–6624.
36 Z. El-Schich, M. Abdullah, S. Shinde, N. Dizeyi, A. Rosén, B. Sellergren and A. Gjörloff Wingren, *Tumor Biol.*, 2016, **37**, 13763–13768.
37 Y. Ma, Y. Yin, L. Ni, H. Miao, Y. Wang, C. Pan, X. Tian, J. Pan, T. You, B. Li and G. Pan, *Bioact. Mater.*, 2021, **6**, 1308–1317.